Cerebral blood flow evaluation of arteriovenous malformations with stable xenon CT.

M P Marks, J O'Donahue, J I Fabricant, K A Frankel, M H Phillips, R L DeLaPaz and D R Enzmann

AJNR Am J Neuroradiol 1988, 9 (6) 1169-1175
http://www.ajnr.org/content/9/6/1169

Cerebral Blood Flow Evaluation of Arteriovenous Malformations with Stable Xenon CT

Michael P. Marks[1]
James O'Donahue[1]
Jacob I. Fabricant[2]
Kenneth A. Frankel[2]
Mark H. Phillips[2]
Robert L. DeLaPaz[1]
Dieter R. Enzmann[1]

Twenty patients with supratentorial arteriovenous malformations (AVMs) were evaluated with angiography, conventional CT, and stable xenon CT to determine cerebral blood flow. Contralateral and ipsilateral regions of interest relative to the AVM were evaluated from cerebral blood flow maps and correlated with angiography. A significant decrease in cerebral blood flow was observed in the ipsilateral cortical gray matter adjacent to the AVM relative to the corresponding contralateral cortex (mean difference = 9.52 ml/100 g/min, $p < .01$). The larger AVMs (>8 cm^3) were associated with a more marked decrease with a mean difference of 12.22 ml/100 g/min ($p < .02$). Regions of interest were also chosen on the basis of angiographic findings, which suggested areas of decreased flow. Comparison of these areas with analogous contralateral areas also showed a significant decline in cerebral blood flow (mean difference = 8.86 ml/100 g/min); this decline was greater with larger AVMs (volume > 8 cm^3), which had a mean difference of 11.38 ml/100 g/min ($p < .01$).

Our correlative study enabled us to pinpoint the regions most likely to have reduced flow from an AVM.

Arteriovenous malformations (AVMs) have been shown to be functionally low-resistance shunts bypassing the normal capillary vascular bed in brain parenchyma [1]. The serious hemorrhagic complications of AVMs are well known, but the physiologic and clinical consequences of hemodynamic disturbances resulting from a high-flow shunt are less well understood. It is difficult to prove an indisputable association between clinical symptoms and the possible diversion of blood flow by an arteriovenous shunt with resulting ischemia. However, many of the complications of AVMs including seizures, progressive neurologic deficits, and intellectual-emotional deterioration are possibly attributable to a "steal" phenomenon [2]. This study was undertaken to both quantify and more accurately localize the most likely regions of decreased flow with AVMs. To achieve these aims the results of flow studies were analyzed by using rigidly defined anatomic regions of interest (ROIs); these were coordinated with angiographic results obtained at the same time in each patient.

Subjects and Methods

Twenty patients, seven males and 13 females, 11–59 years old (mean, 35.5 years), with known supratentorial AVMs were evaluated at Stanford Medical Center for possible therapy with helium ion Bragg peak radiosurgery [3]. All patients underwent cerebral angiography, nonenhanced CT of the brain, and cerebral blood flow (CBF) evaluation with stable xenon CT during the same admission. Some of the patients had a prior history of intracranial hemorrhage, but no patient was examined with an acute or subacute hemorrhage. In addition, patients with previous surgical or embolization therapy that might alter blood flow analysis were eliminated from the study.

All angiograms were selective internal carotid and vertebral artery injections. A stereotactic frame was used to provide reproducible positioning (±2 mm) and magnification. The central

Received August 10, 1987; accepted after revision March 16, 1988.

[1] Department of Diagnostic Radiology and Nuclear Medicine, S–072, Stanford University School of Medicine, Stanford, CA 94305. Address reprint requests to M. P. Marks.

[2] Donner Pavilion and Donner Laboratory, University of California, Berkeley, Berkeley, CA 94720.

AJNR 9:1169–1175, November/December 1988
0195–6108/88/0906–1169

nidus of the AVM was outlined on both lateral and anteroposterior projections. The diameters of the AVM nidus were then determined in three orthogonal planes (craniocaudad, dorsoventral, and mediolateral). An estimate of the volume was determined by multiplying the measurements from the three orthogonal planes together. Larger, irregularly shaped AVMs were divided into smaller components for volume determination.

All the patients were evaluated with a GE 9800 CT scanner fitted with an integrated hardware and software CBF system designed specifically for the scanner. Initial nonenhanced images (slice thickness, 10 mm) were used to select two axial levels, one through the thalamus and basal ganglia, and one through the centrum semiovale. A 33% xenon/67% oxygen gas mixture was used. Blood flow calculations were used to generate high-resolution blood flow maps. Details of the computational methodology have been described [4, 5].

The conventional CT images at each level were then used as a template to draw anatomic ROIs on the CBF maps (Figs. 1 and 2). The regions analyzed included the cortex, larger vascular territories (anterior, middle, and posterior cerebral arteries), and deep gray-matter areas (thalamus, caudate, and lenticular nuclei). An adjacent cortex was assigned on the basis of proximity to the AVM nidus and is indicated for each patient in Table 1. In three patients (cases 9, 15, and 17), the neighboring adjacent cortex was chosen because the vascular nidus extended to the cortical gray matter and caused a marked increase in the local CBF for that region. Cortical areas of potential compromise representing the distal vascular territory of arteries that first fed the AVM were identified from the angiogram. These are listed in the last column of Table 1 as regions of predicted decreased flow. The mean CBF for a particular ROI on the side ipsilateral to the AVM was subtracted from the same ROI in the contralateral hemisphere. This yielded a mean difference of CBF in every patient for each of the anatomically defined ROIs.

Results

Table 1 summarizes clinical manifestations and angiographic findings. AVM volumes ranged from 1 to 20 cm^3 (mean, 8.65 cm^3). All the AVMs were supratentorial: five were in the occipitoparietal region; four in the parietal lobe; four in the temporal lobe; two in the basal ganglia; and one each in

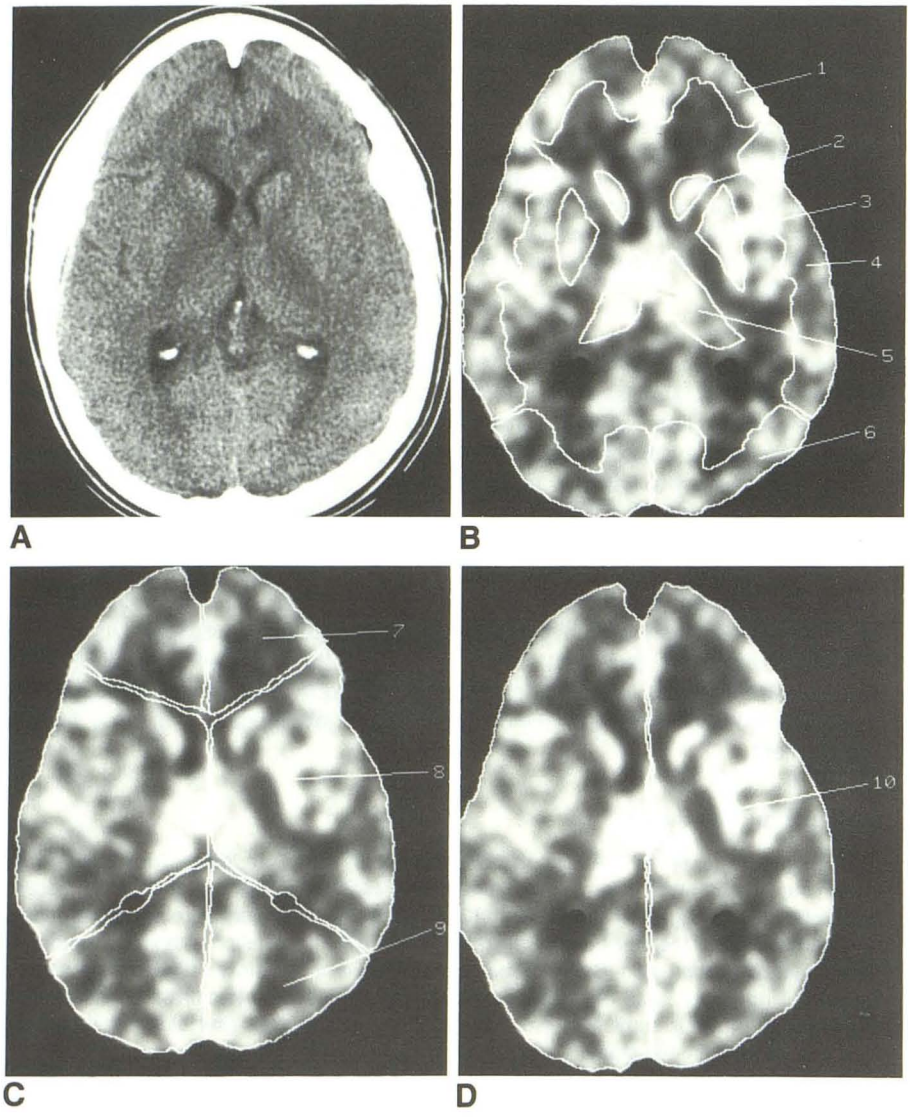

Fig. 1.—*A*, Conventional CT scan through level of thalamus and basal ganglia.

***B–D*, Corresponding xenon cerebral blood flow maps with regions of interest outlined (areas of increased intensity are higher flow). 1 = frontal cortex; 2 = head of caudate; 3 = lenticular nucleus; 4 = sylvian cortex; 5 = thalamus; 6 = occipital cortex; 7 = anterior cerebral artery territory; 8 = middle cerebral artery territory; 9 = posterior cerebral artery territory; 10 = hemisphere.**

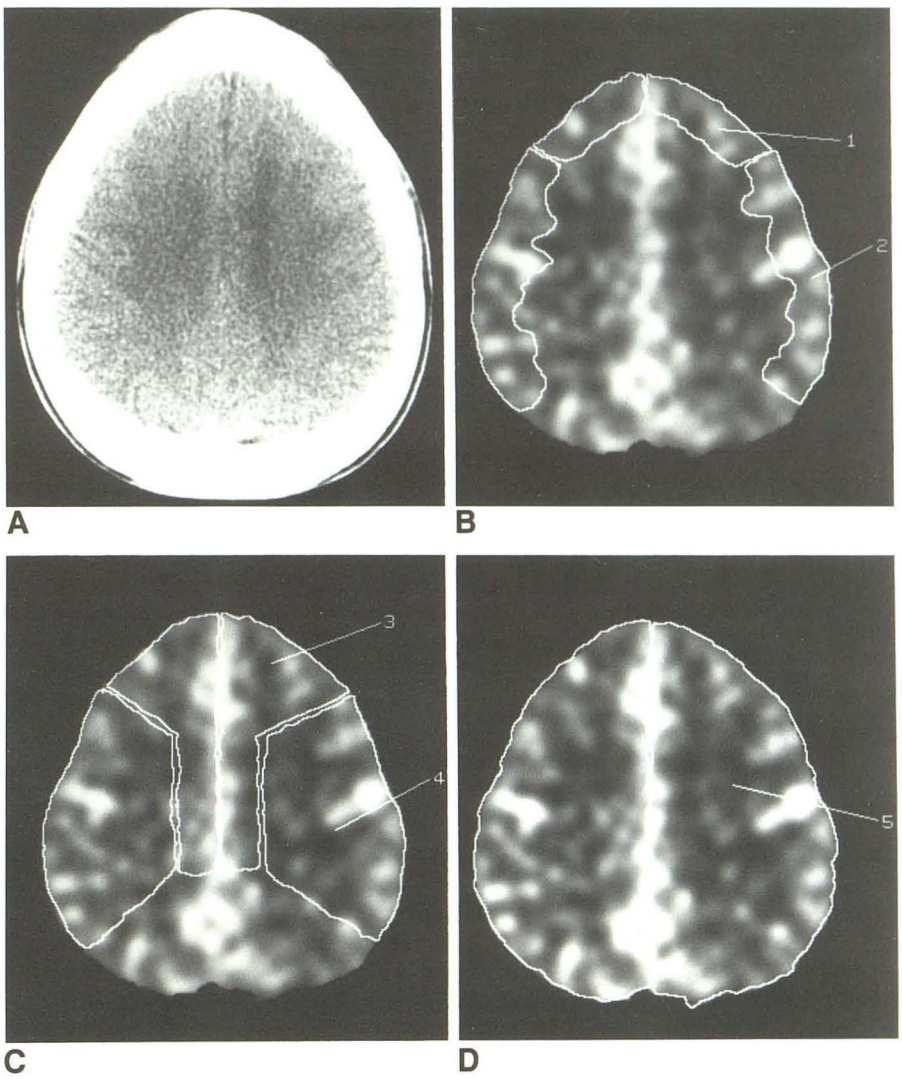

Fig. 2.—*A*, Conventional CT scan through level of centrum semiovale.

***B–D*, Corresponding xenon cerebral blood flow maps with regions of interest outlined: 1 = frontal cortex; 2 = parietal cortex; 3 = anterior cerebral artery territory; 4 = middle cerebral artery territory; 5 = hemisphere.**

the occipital lobe, thalamus, choroid plexus of lateral ventricular atrium, quadrigeminal cistern, and frontoparietal region. Six lesions were right-sided and 14 were left-sided.

Pertinent findings on the nonenhanced CT scans, as they might affect the interpretation of xenon flow studies, are also shown in Table 1. These include regions of calcification, hemorrhage, and encephalomalacia or atrophy. Six of 20 patients showed calcification, but this was limited to the AVM nidus. Five of 20 patients showed small areas of encephalomalacia that did not extend to the cortical region. Two of 20 patients showed mild atrophic change with widening of the sylvian fissure or ventricular enlargement.

An example of the angiographic and postenhancement CT findings in one of the patients is shown in Figure 3, along with the accompanying xenon CBF map generated for this patient. The mean differences in CBF in all patients are shown in Table 2. In most regions no significant difference in CBF was seen between the cortex ipsilateral to the AVM and the contralateral cortex. The exception was the parietal cortex adjacent to the AVM, which showed a significantly lower CBF, with a mean difference of 7.54 ml/100 g/min ($p < .02$). This difference became greater when only larger AVMs (>8 cm^3) were considered. In this group the mean difference in CBF was 10.63 ml/100 g/min ($p < .01$).

Table 3 shows the mean differences in CBF when the cortex directly adjacent to the AVM was compared with the contralateral cortex. It also shows the mean difference for those cortical regions that would have a predicted decrease in flow based on the angiographic results. Sixteen of 20 patients had a lower CBF in the ipsilateral adjacent cortex when compared with the contralateral cortex of the same region, with a mean difference of 9.52 ml/100 g/min ($p < .01$). This difference was greater with larger AVMs (12.22 ml/100 g/min, $p < .02$). Fifteen of 19 patients whose angiograms predicted a decreased CBF had a lower CBF in the ipsilateral cortical regions (8.86 ml/100 g/min, $p < .01$). This difference was greater with the larger AVMs (11.38 ml/100 g/min, $p < .01$). The CBF in larger vascular territories (e.g., middle cere-

TABLE 1: Clinical, Angiographic, and CT Findings in Patients with Arteriovenous Malformations (AVMs)

Case No.	Age	Gender	Clinical Manifestations	AVM Location	Angiographic Findings		CT Findings[a]	Cortex Adjacent to AVM	Location of Predicted Steal[b]
					Volume (cm^3)	Major Feeding Vessels (Territory)			
1	15	F	R focal motor seizures	L parietal	6	Pericallosal, callosomarginal, opercular (ACA, MCA)	None	Parietal	Parietal, high frontal
2	34	M	Generalized seizures	L posterior temporal	4	Inferior temporal (PCA)	None	Parietal	Occipital
3	31	F	Headaches	R parietal	2	Opercular (MCA)	None	Parietal	Parietal
4	55	F	R hemiparesis, transitory aphasia	L parietal	9	Opercular (MCA)	Focal Ca in region of AVM nidus	Parietal	Parietal
5	32	F	Headaches, IVH 6 months before	R thalamic	14	Thalomoperforating, medial posterior choroidal, lateral posterior choroidal (PCA)	None	Sylvian	Occipital
6	59	F	Headache	L basal ganglia	3	Medial lenticulostriate (MCA)	Ca in L caudate, lenticular nucleus; widening of L sylvian fissure	Sylvian	Sylvian, parietal
7	32	F	Intracerebral hemorrhage 4 years and 6 months before	R temporal	9	Inferior temporal (PCA), anterior and posterior temporal (MCA)	LDA in L temporal, frontoparietal lobe	Sylvian	Sylvian, parietal
8	11	M	Intracerebral hemorrhage 2 months before	R occipital	12	Parietooccipital, calcarine (PCA)	None	Occipital	Occipital
9	32	F	Generalized seizures	L temporal (extending to sylvian cortex)	20	Anterior and posterior temporal (MCA)	None	Parietal	Parietal
10	31	F	R visual field deficit; hemorrhage at ages 15 and 22	L occipitoparietal	9	Opercular, angular (MCA), parietooccipital (PCA)	None	Parietal, occipital	Parietal, occipital
11	39	M	Seizures	L parietal	4	Posterior parietal, angular (MCA)	None	Parietal	Parietal
12	36	M	Seizures	L occipitoparietal	9	Opercular, angular (MCA), parietooccipital (PCA)	Focal Ca in region of AVM nidus; LDA in periventricular WM adjacent to AVM nidus	Parietal, occipital	Parietal, occipital
13	39	F	L visual field defect, prior parenchymal hemorrhage, headache	R occipitoparietal	1	Calcarine, parietooccipital (PCA)	Small LDA in WM of parietal lobe	Parietal, occipital	Occipital
14	38	M	L third nerve palsy, headaches	L quadrigeminal cistern	1	Medial posterior choroidal (PCA)	Very small LDA in L tectum	Occipital	Occipital
15	45	M	Partial complex and generalized seizures	L temporal (extends to sylvian cortex)	12	Anterior and posterior temporal (MCA), inferior temporal (PCA)	Ca in region of AVM nidus	Parietal	Occipital, parietal
16	40	F	Headaches, IVH 8 months before	L lateral ventricle, choroid plexus	2	Distal pericallosal (ACA)	None	Occipital	None
17	35	F	Headaches, L arm numbness	R occipitoparietal (extends to occipital cortex)	16	Opercular, angular (MCA)	None	Parietal	Parietal
18	25	M	Generalized seizures	L occipitoparietal	12	Angular (MCA), parietooccipital, inferior temporal (PCA)	None	Parietal, occipital	Parietal, occipital
19	37	F	Parenchymal hemorrhage and IVH 1 year before	L basal ganglia	9	Thalamoperforating, lateral posterior choroidal (PCA)	Ca in L basal ganglia; slight enlargement in L lateral ventricle	Sylvian	Occipital
20	43	F	Generalized seizures	L frontoparietal	16	Operculofrontal (MCA), pericallosal, callosomarginal (ACA)	Focal Ca in AVM nidus; small LDA in surrounding region of nidus	High frontal, parietal	High frontal, parietal

Note.—R = right; L = left; ACA = anterior cerebral artery; MCA = middle cerebral artery; PCA = posterior cerebral artery; Ca = calcification; IVH = intraventricular hemorrhage; LDA = low-density area; WM = white matter.

[a] Evaluation for calcification, hemorrhage, encephalomalacia, or atrophy (see text for explanation).

[b] See text for explanation.

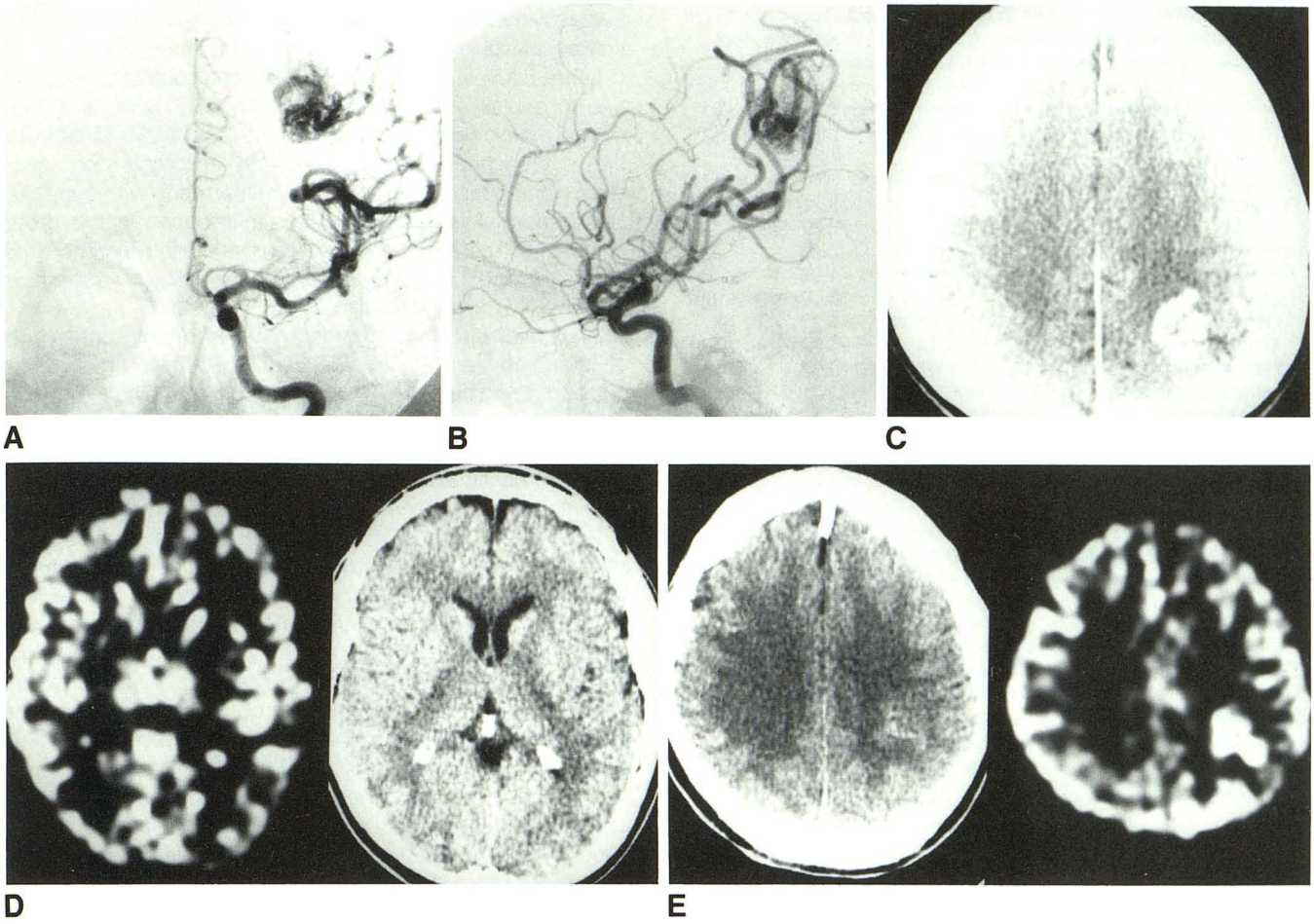

Fig. 3.—Left parietal arteriovenous malformation (case 11) shows decreased flow in adjacent cortex with xenon cerebral blood flow map.

***A–C*, Anteroposterior and lateral internal carotid angiograms and postenhancement CT scan, respectively, show nidus of malformation with supply from branches of left middle cerebral artery. Therefore, parietal cortex was both the adjacent cortex and the location of predicted steal.**

***D* and *E*, Conventional xenon-enhanced CT scans and xenon cerebral blood flow maps for two axial levels. Area of increased flow in higher cut (*E*) corresponds to actual nidus of malformation; region of decreased flow in adjacent parietal cortex is seen at same level. Cerebral blood flow calculated from region of interest for right parietal cortex was 73 ml/100 g/min; for left parietal cortex adjacent to malformation it was 48 ml/100 g/min.**

bral artery territory, anterior cerebral artery territory, or an entire hemisphere) showed no significant difference when ipsilateral and contralateral sides were compared.

For the entire group of patients the mean CBF (including all gray- and white-matter structures) at the lower axial level through the thalamus and basal ganglia was 50.18 ± 14.24 ml/100 g/min. At the upper axial cut through the centrum semiovale the mean CBF was 44.38 ± 12.27 ml/100 g/min. The mean CBF for all the cortical regions measured was 51.68 ± 18.3 ml/100 g/min.

Discussion

Initial attempts to assess the hemodynamic alterations caused by AVMs focused on the actual shunt flow by using inert gas diffusion with injected xenon-133 or krypton-85 [6, 7] and inhaled xenon-133 [8]. Feindel et al. [9], with the use of fluorescein angiography and diffusible and nondiffusible radiotracers, reported improved blood flow in uninvolved regions of the brain after ligation of the main vessels feeding a temporal-lobe AVM, providing evidence for the presence of "cerebral steal."

More recently, other authors [10–12] have used different methods to show variable decreases in blood flow in parenchyma adjacent to and in some cases far removed from the AVM. Takeuchi et al. [10] examined six patients with three radiotracers and single-photon emission CT (SPECT) to evaluate flow in cases of AVMs. The AVMs were not measured but described as small, medium, and large, and regardless of size they showed regions of decreased activity in the ipsilateral hemisphere. These data were not correlated with angiographic results and quantitative CBF, but qualitative focal decreases were noted. Two recent studies that quantitated CBF have shown variable results in terms of the areas of involvement. Homan et al. [11] used xenon-133 SPECT to show "steal areas" in eight of 11 AVM patients who were compared with a group of normal controls. These regions, however, appeared to be randomly located in the contralateral and ipsilateral hemispheres and in areas of arterial supply that

TABLE 2: Mean Differences in Cerebral Blood Flow (Contralateral Minus Ipsilateral)

Level: Region	Mean Difference (ml/100 g/min)		
	Volume ≤ 8 cm^3	Volume > 8 cm^3	Total
Thalamus and basal ganglia:			
Anterior cerebral artery	0.74	3.26	2.25
Middle cerebral artery	−3.32	−5.67	−4.73
Posterior cerebral artery	−1.27	−2.86	−2.22
Frontal cortex	1.07	−4.99	−2.56
Sylvian cortex	−3.40	−6.70	−5.38
Occipital cortex	−1.07	4.93	2.53
Thalamus	5.14	−4.22	−0.48
Head of caudate	−7.98	−6.53	−7.11
Lenticular nucleus	2.01	−5.31	−2.38
Hemisphere	−3.27	−4.44	−3.97
Centrum semiovale:			
Anterior cerebral artery	0.70	−1.83	−0.82
Middle cerebral artery	−0.51	2.65	1.38
Frontal cortex	1.07	−4.99	−2.56
Parietal cortex	2.91	10.63	7.54
Hemisphere	0.52	1.58	1.16

TABLE 3: Mean Differences in Cerebral Blood Flow (Contralateral Minus Ipsilateral) for Cortices Adjacent to Arteriovenous Malformation and Cortices with Predicted Decreased Flow

Region of Interest	Mean Difference (ml/100 g/min)		
	Volume ≤ 8 cm^3	Volume > 8 cm^3	Total
Cortex adjacent to arteriovenous malformation	5.48[a]	12.22[b]	9.52[c]
Cortex with predicted decrease in flow	4.55[a]	11.38[c]	8.86[c]

[a] Not significant.
[b] $p < .02$.
[c] $p < .01$.

were not directly related to the AVM. Okabe et al. [12] used stable xenon CT and measured CBF in small ROIs in gray and white matter. The data were not correlated with size or angiographic results, but a significant decrease in CBF in gray and white matter adjacent to the AVM was found when compared with that of normal controls. In addition, contralateral gray matter demonstrated a smaller decrease (still statistically significant) when compared with normals.

Previous studies that used stable xenon CT [13] and xenon-133 SPECT [14] to measure CBF in normal patients have shown very little interhemispheric difference regardless of the region measured, including selected regions of cortical gray matter. These results were also seen in our patients, with no significant difference observed when comparing right and left sides in ROIs not related to the AVM. We have shown that cortical areas adjacent to AVMs or cortical areas selected on the basis of angiographic decreased flow have a reduced CBF when compared with the analogous region on the contralateral side. Larger ROIs such as major vascular territories (anterior, middle, or posterior cerebral artery territory) or the entire hemisphere showed no significant difference.

Other causes could exist in a patient population such as this to explain regional decreases in CBF besides a local hemodynamic response to the shunt of an AVM. Most notably, subarachnoid hemorrhage with accompanying vasospasm and possibly parenchymal hemorrhage with compression of normal vascular structures might occur in this group of patients. There was no evidence of acute intraparenchymal or subarachnoid hemorrhage and no evidence of vasospasm on either CT or angiography.

It has been shown that cortical regions distant from an area of infarction can display reduced blood flow [15, 16]. In addition, positron emission tomographic scanning in patients with brain tumors has shown suppression of gray-matter glucose use in regions spatially remote from the lesion [17]. These three studies suggest functional changes in cortical gray matter remote from regions of disease, which may reflect a decrease in CBF. Examining 10 cases of internal capsular infarct Takeno et al. [16] found a significant decrease in mean CBF in adjacent cortical regions and a tendency for the flow to drop off with larger infarcts. It was their belief that this remote effect, which they termed *intracerebral diaschisis*, might be caused by the dropout of afferent and efferent fibers passing through the region of infarct. AVMs cause damage to surrounding tissue seen as low density on CT and high signal on T2-weighted MR images. Pathologic examination of such areas in the interstices of AVMs and adjacent to them usually shows gliotic tissue [18]. Therefore, disruption of fiber tracts by an AVM nidus is possible and could cause intracerebral diaschisis. While size-related CBF changes can be explained by the presence of a larger shunt and hence more significant CBF decrease, it is also true that larger AVM nidi will cause more gliotic change.

Not all patients showed a significant regional decrease in CBF adjacent to the AVM. Enlarged feeding and draining vessels are often noted adjacent to an AVM nidus, and many of these traverse the cortical gray matter. These vessels could be included in the ROI, potentially spuriously elevating CBF measurements, so that in selected cases (particularly those cases that feed or drain from lateral cortical margins) there may be elevation of CBF in adjacent cortical regions. Our selection of cortical gray-matter ROIs minimized this error.

It is unclear how many patients with AVMs have symptoms from a steal phenomenon. Clearly, many AVMs do not produce ischemic symptoms, and, given the magnitude of the CBF decrease seen in our patients and reported by others, this is not surprising. The mean CBF for all the cortical regions measured was 51.68 ± 18.3 ml/100 g/min. We have demonstrated a statistically significant drop in cortical blood flow in selected cortical regions in the range of approximately 8–12 ml/100 g/min. It has been shown that normal electrophysiologic activity is maintained with a CBF as low as 15–20 ml/100 g/min [19], which is well below the level measured in any of our ROIs. In the resting state for our measurements we demonstrated a "steal" of blood or reduction in cerebral blood

from selected adjacent cortex. However, this decrease in blood flow did not appear to be great enough to result in symptomatic ischemia.

ACKNOWLEDGMENT

We thank Margaret Tuggle for valuable assistance in manuscript preparation.

REFERENCES

1. Nornes H, Grip A. Hemodynamic aspects of cerebral arteriovenous malformations. *J Neurosurg* **1980**;53:456–464
2. Kusske JA, Kelly WA. Embolization and reduction of the "steal" syndrome in cerebral arteriovenous malformations. *J Neurosurg* **1974**;40:313–321
3. Fabrikant JI, Lyman JT, Hosobuchi Y. Stereotactic heavy-ion Bragg peak radiosurgery for intra-cranial vascular disorders: method for treatment of deep arteriovenous malformations. *Br J Radiol* **1984**;57:479–490
4. Yonas H, Good WF, Gur D. Mapping cerebral blood blow by xenon-enhanced computed tomography: clinical experience. *Radiology* **1984**;152:435–442
5. Gur D, Wolfson SK, Yonas H, et al. Progress in cerebrovascular disease: local cerebral blood flow by xenon enhanced CT. *Stroke* **1982**;13:750–758
6. Haggendal E, Ingvar DH, Lassen NA, et al. Pre- and postoperative measurements of regional cerebral blood flow in three cases of intracranial arteriovenous aneurysms. *J Neurosurg* **1965**;22:1–6
7. Lassen NA, Munck O. Cerebral blood flow in arteriovenous anomalies of the brain determined by the use of radioactive krypton 85. *Acta Psychiatr Scand* **1956**;31:71–80
8. Menon D, Weir B. Evaluation of cerebral blood flow in arteriovenous malformations by the xenon 133 inhalation method. *Can J Neurol Sci* **1979**;6:411–416
9. Feindel W, Yamamoto YL, Hodge CP. Red cerebral veins and the cerebral steal syndrome. Evidence from fluoroscein angiography and microregional blood flow by radioisotopes during excision of an angioma. *J Neurosurg* **1971**;35:167–179
10. Takeuchi S, Kikuchi H, Karasawa J. Cerebral hemodynamics in arteriovenous malformations: evaluation by single-photon emission CT. *AJNR* **1987**;8:193–197
11. Homan RW, Devous MD, Sokely EM, Bonte FJ. Quantification of intracerebral steal in patients with arteriovenous malformation. *Arch Neurol* **1986**;43:779–785
12. Okabe T, Meyer JS, Okayasu H. Xenon-enhanced CT CBF measurements in cerebral AVMs before and after excision. *J Neurosurg* **1983**;59:21–31
13. Tachibana H, Meyer JS, Okayasu H, Kandula P. Changing topographic patterns of human cerebral blood flow with age measured by xenon CT. *AJNR* **1984**;5:139–146
14. Shirata N, Henriksen L, Vorstrup S, et al. Regional cerebral blood flow assessed by ^{133}Xe inhalation and emission tomography; normal values. *J Comput Assist Tomogr* **1985**;9:861–866
15. Celesia G, Polcyn R, Holden J, Nickles R, Koeppe R, Gatley S. ^{18}F-fluoromethane positron emission tomography determination of regional cerebral blood flow in cerebral infarction. *J Cereb Blood Flow Metab* **1983**;3[Suppl 1]:23–24
16. Takano T, Kimura K, Nakamura M, et al. Effects of small deep hemispheric infarction on the ipsilateral cortical blood flow in man. *Stroke* **1985**;16:64–69
17. DeLaPaz RL, Patronas NJ, Brooks RA, et al. Positron emission tomographic study of suppression of gray-matter glucose utilization by brain tumors. *AJNR* **1983**;4:826–829
18. Stein B, Wolpert SM. Arteriovenous malformations of the brain: current concepts and treatment. *Arch Neurol* **1980**;37:1–5
19. Astrup J, Symon L, Branston NM, Lassen NA. Cortical evoked potential and extracellular K^+ and H^+ at critical levels of brain ischemia. *Stroke* **1977**;8:51–57